sciendo

ARTIFICIAL SATELLITES, Vol. 57, No. 2 – 2022
DOI: 10.2478/arsa-2022-0006

A SCRIPT-DRIVEN APPROACH TO MAPPING SATELLITE-DERIVED TOPOGRAPHY AND GRAVITY DATA OVER THE ZAGROS FOLD-AND-THRUST BELT, IRAN

Polina LEMENKOVA

Université Libre de Bruxelles, École polytechnique de Bruxelles, Brussels, Belgium

e-mails: polina.lemenkova@ulb.be, pauline.lemenkova@gmail.com

ABSTRACT. Integrated geophysical mapping benefits from visualizing multi-source datasets including gravity and satellite altimetry data using 2D and 3D techniques. Applying scripting cartographic approach by R language and GMT supported by traditional mapping in QGIS is presented in this paper with a case study of Iranian geomorphology and a special focus on Zagros Fold-and-Thrust Belt, a unique landform of the country affected by complex geodynamic structure. Several modules of GMT and 'tmap' and 'raster' packages of R language were shown to illustrate the efficiency of the console-based mapping by scripts. Data sources included high-resolution raster grids of GEBCO/SRTM, EGM-2008, SRTM DEM and vector geologic layers of USGS. The cartographic objective was to visualize thematic maps of Iran: topography, geology, satellite-derived gravity anomalies, geoid undulations and geomorphology. Various cartographic techniques were applied to plot the geophysical and topographic field gradients and categorical variations in geological structures and relief along the Zagros Fold-and-Thrust Belt. The structures of Elburz, Zagros, Kopet Dag and Makran slopes, Dasht-e Kavir, Dasht-e Lut and Great Salt Desert were visualized using 3D-and 2D techniques. The geomorphometric properties (slope, aspect, hillshade, elevations) were modelled by R. The study presented a series of 11 new maps made using a combination of scripting techniques and GIS for comparative geological-geophysical analysis. Listings of R and GMT scripting are provided for repeatability.

Keywords: geophysics, cartography, R, GMT, satellite altimetry

1. INTRODUCTION

1.1. Background and motivation

Cartographic visualization based on spatial data represents a successful approach in geological and topographic modelling. Mapping plays a significant role in a wide range of applications, including natural resource management, mineral exploration, geophysical risk assessment and so on. It is well known that real-world geologic applications, such as modelling, prognosis, reconstruction and resource assessment, require precise maps and models. It therefore becomes crucial to test and apply novel cartographic methods and techniques to map topographic, geological and geophysical datasets. It is commonly accepted that designing effective maps and their 3D models has to balance between the robustness and availability of data, the convenience

© The Author(s). This is an open-access article distributed under the terms of the Creative Commons Attribution License (CC BY 4.0, https://creativecommons.org/licenses/by/4.0/), which permits use, distribution, and reproduction in any medium, provided that the Article is properly cited.

of technical mapping routine and the robustness of maps. Previous works on using scripts in cartography have shown the effectiveness of data automation in various issues, such as interpolated DEM (Shi et al., 2009), semantic data modelling, (Gedicke et al., 2021; Kasalica and Lamprecht, 2018), precise bathymetric modelling (Virden et al., 2004), image processing Andreo et al. (2015); Lemenkova (2021a); Senturk et al. (2016), environmental monitoring (De Sarkar et al., 2012) and spatial computing (Hrovat et al., 2013; Huang et al., 2007; Lemenkova, 2022b), which can illustrate the increased functionality of scripting through automation of mapping.

1.2. Study area

This study focuses on the geomorphological 2D and 3D mapping of the Zagros Fold-and-Thrust Belt in Iran using scripting cartographic techniques (Figure 1).

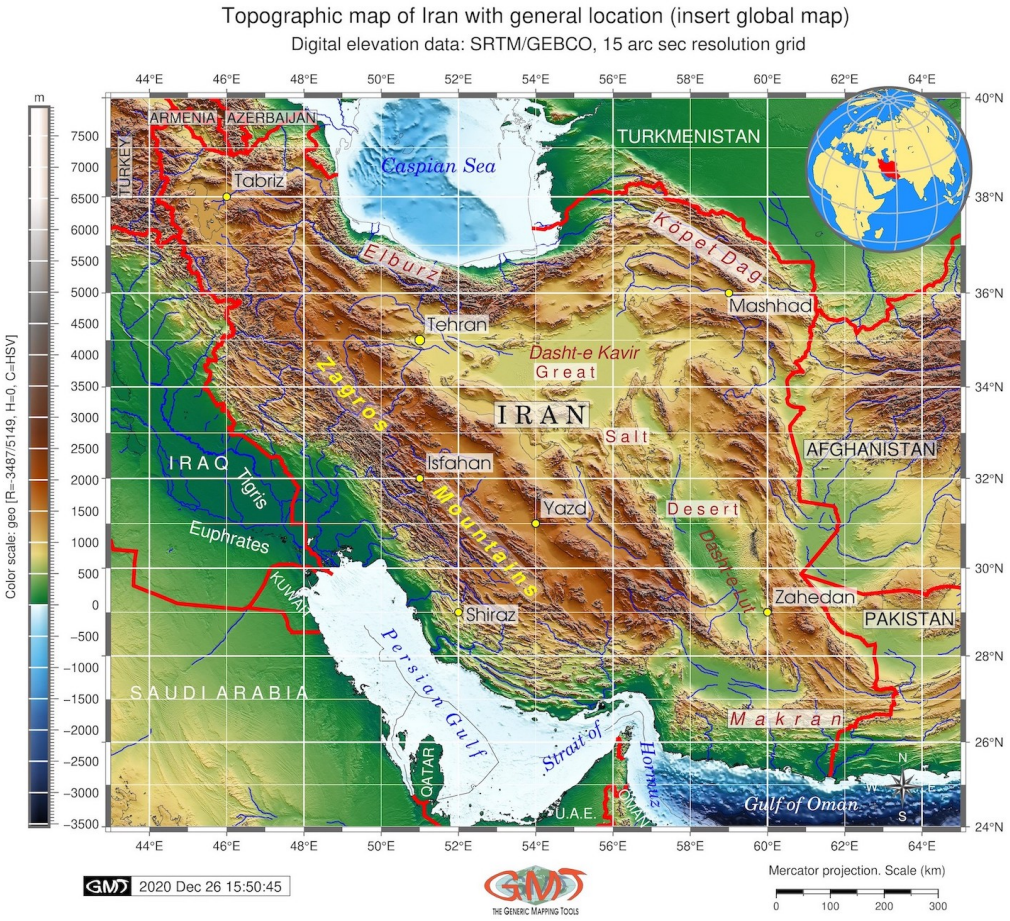

Figure 1. Topographic map of Iran. Data source: *General Bathymetric Chart of the Oceans (GEBCO)*, GEBCO Compilation Group (2020). Mapping in GMT.

The Zagros Fold-and-Thrust Belt is a major orogenic landform of Iran located in the northern part of the Arabian plate, a part of the Alpine–Himalayan orogenic belt, and a location for Zagros phosphogenic horizon, hosted by the Eocene-Oligocene Pabdeh Formation (Zarasvandi et al., 2021). Geologically, it was formed as a result of the collision between the Arabian and central Iran tectonic plates (Jahani et al., 2009). The observed variations in geomorphology of Zagros mountains is a primary indicator of geologic and tectonic processes leading to its landform formation. The shape of the modern topography of the Zagros Fold-and-Thrust Belt reflected in the basin's structural division results from the regional tectonic and sedimentary evolution

involving deep interactions between the Earth's crust, mantle and sub-surface geologic processes occurring since Quaternary.

Variations in geomorphic structures of the Zagros Fold-and-Thrust Belt system are a significant indicator of the distribution of mineral resources, since Zagros region belongs to the key basins of the oil and gas reserves in the Middle East, e.g., with prolific petroleum fields in the Zagros Foreland (Bosold et al., 2005). The giant oil and gas reserves of Zagros region are indicated by regional tectonic and sedimentary evolution, basin structural division, petroleum distribution characteristics and main controlling factors of petroleum accumulation. For instance, the Piranj oil field is a part of the Middle Cretaceous–Early Miocene Petroleum System in Zagros basin and southwest of Iran (Elyasi, 2016).

The oil fields are mainly located in the foredeep zone, while gas fields are predominantly in the simply folded zone and few fields are in the Zagros thrust fault zone (Liu et al., 2018). The spatial geological structure of the Zagros Basin differs from southwest to northeast dividing the basin into the three major zones: foredeep, simply folded and thrust fault. Spatial differences in geological structure are reflected in the distribution of mineral deposits: the oil fields are mostly located in the foredeep zone, gas fields – in the simply folded zone and only few fields are in the thrust fault zone. The belt of prolific oil and gas fields is bounded on the northeast by the high Zagros mountains and on the south and west by the outcropping crystalline basement of the Arabian Shield (Beydoun et al., 1992).

The Zagros orogenic belt of Iran consists, from northeast to southwest, of the parallel tectonic subdivisions with the increased intensity of deformation northeast from the Persian Gulf-Mesopotamian basin: (1) the Urumieh-Dokhtar Magmatic Assemblage; (2) the Sanandaj-Sirjan Zone; and (3) the Zagros Simply Folded Belt (Alavi, 1994). Enhanced understanding of the geologic and tectonic processes taking place in Zagros Fold-and-Thrust Belt, and the role of these processes in distribution of mineral resources of Iran, is vital for improving both geologic prognosis and predictions of oils and gas plays, and for environmental modeling aimed at regional geomorphological and applied geologic analysis: water runoff, landslide monitoring, earthquake and seismic mapping.

1.3. Related works

Mapping Iran using advanced techniques and robust data is largely inspired by corresponding geological work on Zagros. In particular, recent cartographic examples of mapping Iran highlight the variable environment and vegetation in the country (Eskandari and Ali Mahmoudi Sarab, 2022; Toosi et al., 2022), point at the richness of its geological resources (Garajeh et al., 2022) and also show the risk of natural hazards (Mafi-Gholami et al., 2022; Mostafa Mousavi et al., 2022). More examples of recent studies focus on regional geologic analysis of Zagros and Makran and the comparative analysis of the tectonic structure with respect to geologic evolution of the Zagros Basin. Technical approaches of these studies are diverse. For instance, earlier studies (Bayer et al., 2006; Masson et al., 2007; Palano et al., 2018) focused on active crustal deformation field for the Zagros Fold-and-Thrust Belt continental collision zone by GPS measurement approach; Lemenkova (2020e) used cross-sectional profiles to visualize submarine geomorphology of the Makran Trench. Motaghi, Shabanian, Tatar, Cuffaro and Doglioni (2017) used seismic linear profiling to study the geometry of the Zagros suture across its south segment and the Urumieh–Dokhtar magmatic arc. Adams et al. (2009) and Masson et al. (2005) studied seismicity and earthquakes in the Zagros region using geophysical methods. Many other studies are based on using field geologic and seismic data by means of the traditional GIS.

The existing studies focus on the geological analysis using existing GIS approaches, plotting stratigraphic columns and statistical graphs for spatial data visualization (Koshnaw et al., 2020; Mouthereau et al., 2007), geologic modelling data using *in-situ* experiments Heidari et al. (2021); Hosseini et al. (2021); Lindh and Lemenkova (2022c); Soleimani and Jodeiri Shokri (2016), geochemical data analysis Afzal et al. (2017); Lindh and Lemenkova (2022a); Mokhtari and Sadeghi (2021) and do not deal with a detailed explanation of scripting techniques of the geological mapping. As a consequence, they either lack detailed explanation of the techniques of cartographic data visualization (Tavani et al., 2018) or have limited use of scripting in geologic modelling (Lemenkov and Lemenkova, 2021). The benefits of the conventional methods of GIS-based mapping are that they can assist in straightforward visualization for simple data analysis using spatial features, to the extent that the maps serve as good background for geological data analysis. In addition, mapping by GIS does not require advanced computational skills and can be performed relatively easily. The drawbacks of these approaches are the lack of automation in data processing, which results in long and time-consuming workflow in case of repetitive operations in a cartographic routine which causes difficulties in plotting. The scripting method, in contrast, belongs to the approach with programming background. Distinct from traditional GIS, it also reinforces automation and speed of the mapping process.

Thus, this study presents a combined geomorphological analysis of Zagros region by 2D and 3D modelling using an integrated approach of R programming language and thematic mapping by QGIS and GMT scripting using the existing methods (Lemenkova, 2022a). Utilizing a scripting approach in cartographic visualization of the geological datasets can increase the speed and quality of data processing and help perform a complex geospatial analysis of Zagros Basin based on the multi-source thematic GIS data integrated by R and GMT modeling techniques (Lemenkova, 2019c). These include, for instance, geomorphometric analysis of slope, aspect using DEM and geophysical mapping of 3D visualization.

1.4. Objectives and goals

The goal of this study is to complete a thematic mapping of Iran using robust spatial data and integrated approaches of GMT and GIS by minimizing the human-based routine and maximizing automation of cartographic work. The dataset includes the geologic, geophysical and topographic raster and vector data, as well as satellite-derived gravity grids. In this study, we show that the advantage of cartographic scripting lies in flexible integration of multi-source data, which can vary in resolution, e.g., GEBCO with 15 arc-second, EGM-2008 with 2.5 arc-minute resolution) spatially and temporally. This requires pre-processing of datasets, calibration, projecting and coordinates adjustment for each dataset. In view of this, time-saving techniques of console-based mapping significantly reduces labour time and increases efficiency.

For each target object on the maps, e.g., vector lines, annotations, continuous polygons, bar scale, legend and more, the objective was to select and apply several GMT modules, which were found using a functionality of GMT. Using scripts, the target maps were iteratively plotted to minimize manual cartographic operations. The scripting procedure iterates by each added GMT module with necessary flags, commands and variables. The refinement was performed for the aesthetically adjusted colour palettes and selection of layout. Since direct *in situ* geologic observations and regular fieldwork in Zagros mountains are difficult to perform, open datasets are effective materials for geologic studies. This explains the use of the computer-based methods for geomorphic mapping of Zagros Basin.

In view of this, the main purpose of this study is to apply scripting techniques for the investigation of the geomorphology of the Zagros Basin, which is formed in complex geological, lithological

and tectonic setting. To this aim, the study applied using 2D and 3D modelling by R and GMT scripting languages. A second task was to determine if the application of technically different tools for geospatial analysis (R, GMT and QGIS) can be integrated in a project for effective visualization and modelling of the study area by a combined approach of programming and GIS. Seven different datasets covering Iran including Zagros mountains provided effective data sources for a cartographic analysis of complex geological nature of the Iranian Plate and Zagros.

2. GEOLOGIC BACKGROUND

The Zagros Fold-and-Thrust Belt is one of the world's largest petroleum provinces, which is a ca. 1,800-km long zone of deformed crustal rocks, formed as a result of the collision between the two tectonic plates: the Arabian Plate and the Eurasian Plate. The importance of the Zagros belt can be illustrated by the fact that it contains about 49% of the existing hydrocarbon reserves of the fold and thrust belts (Cooper, 2007). The Zagros Fold-and-Thrust Belt is formed along the line of the oblique convergence of the Arabian Plate, which moves northwards to the Eurasian Plate at a rate of ca. 3 cm/year (Talebian and Jackson, 2004).

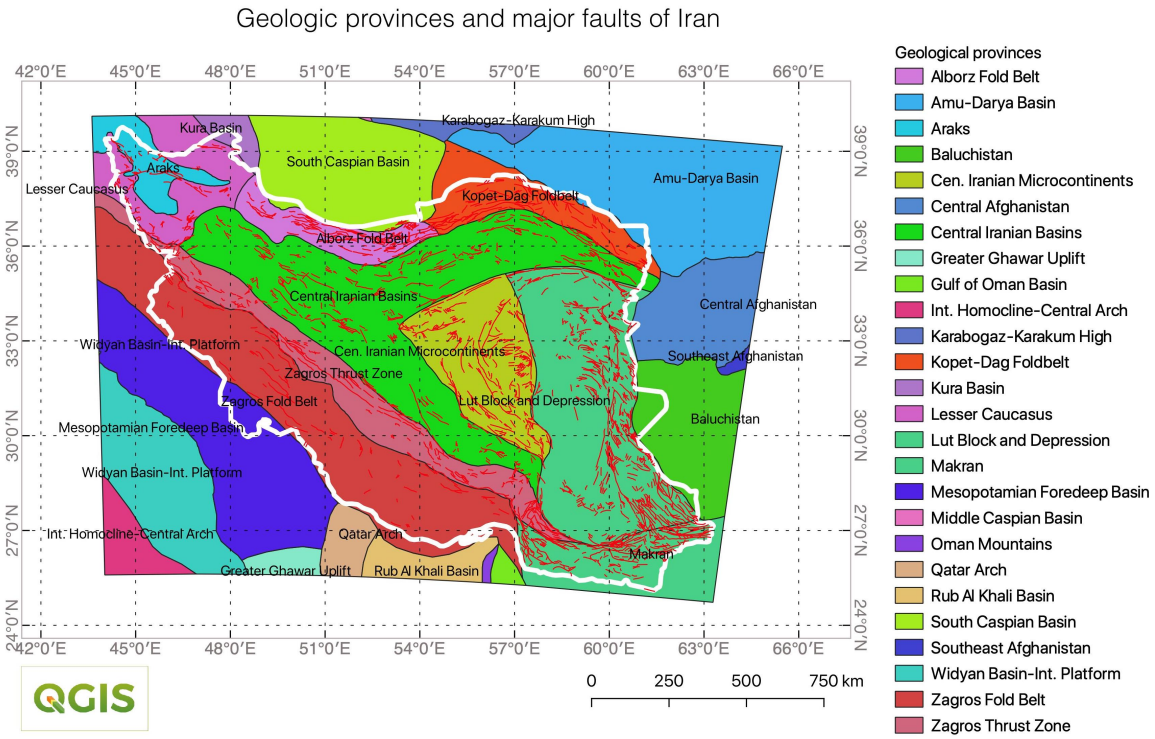

Figure 2. Geologic map of Iran. Data source: *United States Geological Survey (USGS)*. Mapping in QGIS.

The structural geologic complexity of Zagros belt results from the geologic deformation. It can be illustrated by the presence of the out-of-sequence, basement-rooted thrusts, incompetent cover strata or folds superimposed upon the pre-existing structures. It also includes a sequence of heterogeneous latest Neoproterozoic–Phanerozoic sedimentary cover 7–12 km thick strata overlying the Precambrian crystalline basement (Alavi, 2007). The Zagros suture, stretching between the Arabian and Eurasian plates, is directed along a line within southeast Turkey through northern Iraq and southern Iran. Southwest of this suture, the continental margin of the Arabian plate is deformed by folds, thrusts and strike-slip faults within the Zagros mountains. Nowadays, the geologic dynamics in the Zagros mountains continues with the deformation front lying roughly parallel to the Iranian shoreline of the Persian Gulf.

Regional tectonic movements can be illustrated by gradual growth of the Turkish–Iranian Plateau which incorporates the adjacent parts of the Zagros Fold-and-Thrust Belt (Allen et al., 2013).

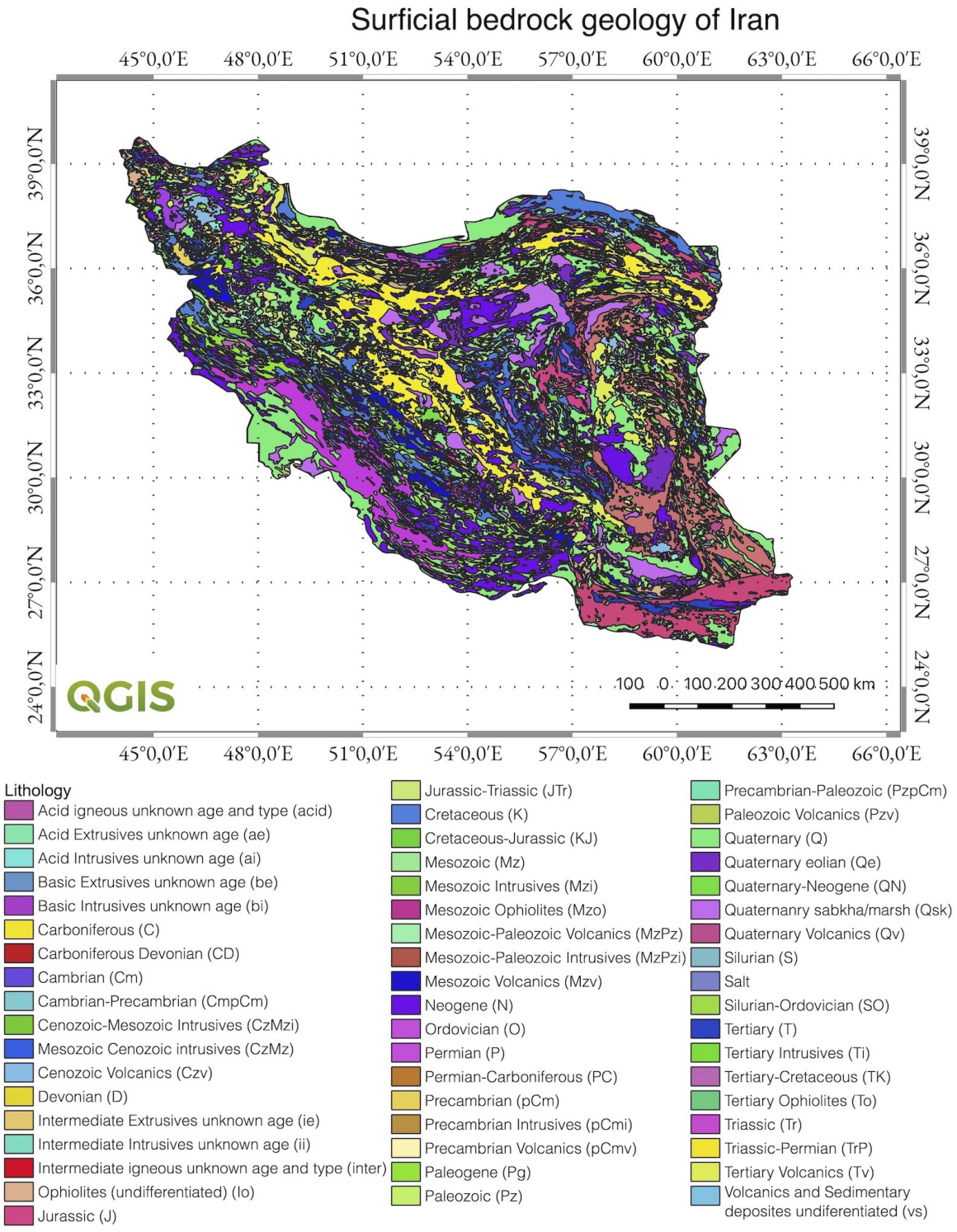

Figure 3. Lithologic map of Iran. Data source: *United States Geological Survey (USGS)*. Mapping in QGIS.

The geologic stratigraphy of Zagros fold-thrust belt has recently been updated and classified as four groups of rocks:

1. Precambrian to Devonian group (the lowest), which consists of several subgroups:

- Neoproterozoic to Cambrian rocks: evaporites, siliciclastic deposits and carbonates;
- Cambrian: shallow, marine siliciclastic and carbonate rocks;
- Ordovician, Silurian, and Devonian shales, siltstones, and volcanogenic sandstones;

2. Permian and Triassic rocks, composed of basal siliciclastic rocks and evaporitic carbonates;
3. Jurassic shallow- and deep-water carbonates from a Neo-Tethyan continental shelf;
4. Cretaceous siliciclastic and carbonate deposits of the Zagros orogen (Alavi, 2004).

A notable part of the geomorphology of Zagros is presented by the Fars arc and thrust belt, propagated under the impact of the Oman Peninsula. The oblique convergence between the Arabic plate and the Iran block mostly extends along the Fars arc (Aubourg et al., 2008). The hydrocarbon production is notable for the Southwest Zagros where oil fields are concentrated. Among others, the Asmari Oligo-Miocene Formation is well-known since it contains a lot of the hydrocarbon reserves of this area (Ahmadhadi et al., 2008). Besides the petroleum resources of Zagros, southern Iran has a remarkable salt plugs segmented by salt diapiric provinces: Hormuz, Shiraz-Kazerun and Nyriz-Jahrum sub-basins, which is connected with the structure and evolution of the Zagros Fold-and-Thrust Belt faulting, as described in details (Bahroudi and Koyi, 2003; Jahani et al., 2009; Khodabakhshnezhad and Arian, 2016).

The tectonics of Zagros has a spatially diverse style with a general trend of northwest–southeast-oriented folds and thrusts, in the simple folded zone, and right-lateral strike-slip on the main recent fault. The fold geometries of Zagros indicate several décollement horizons including shale units, evaporites in the Neogene, Mesozoic, Lower Palaeozoic and upper Proterozoic successions (Blanc et al., 2003). A detailed stratigraphy of the tectonic sub-division of Zagros Suture Zone formed since Cretaceous was reported earlier (Ali et al., 2012, 2014; Authemayou et al., 2006).

The geologic stratigraphy of Zagros mirrors major steps in its evolution that can be briefly characterised as follows. The subduction of the Paleo-Tethys induced the formation of the Zagros Basin, which is caused by intense rifting, evolved in the Jurassic period. The main rocks of the Mesozoic and Cenozoic reservoirs (carbonate, shale and evaporite) are sourced from the continental marginal deposit between the Arabian Shield and Zagros belt, extending to over 1000 km southwards. Nowadays, such particular structural-geomorphological features and topographic fronts at the surface of Zagros are the main regions of earthquakes in Iran (Berberian, 1995). The thrusts, frontal asymmetric anticlines, escarpments and Quaternary deformation mark the topographic fronts on the relief surface of Zagros. They have vertically displaced geologic beds, which highlight a deep correlation between the topographic, geomorphological and geologic structure of Zagros Fold-and-Thrust Belt.

3. MATERIALS AND METHODS

The proposed study is performed using a combination of methods using open source geoinformation tools such as console-based GMT, a graphical user interface (GUI) QGIS and programming language R. Full scripts used for mapping by R and GMT are publicly avaiilable on author's GitHub repository for repeatability in similar studies: https://github.com/paulinelemenkova/Mapping_Iran_R_GMT_Scripts-. The datasets include openly available geospatial raster and vector layers as follows.

1. The topographic map (Figure 1) was based on GEBCO/SRTM (GEBCO Compilation Group, 2020), a high-resolution (15 arc-second) raster grid of the Earth relief. The GEBCO grid has been widely used in geoscience papers where its advantages were used (Lemenkova, 2020a,d, 2021e; Lindh and Lemenkova, 2021a). GEBCO presents a combination of land topography with partially measured and estimated bathymetry using remote sensing data.

2. The geologic mapping (Figure 2) was performed using the datasets of UNESCO, which include petroleum geology, geologic provinces and oil and gas fields of Iran. This dataset is a cartographic part of the worldwide series released by the U.S.G.S. World Energy Project obtained in shape (.shp) file format and processed using QGIS.

3. The lithology of Iran (Figure 3) is mapped using the datasets of UNESCO on surficial geology, which includes the petroleum geology, geologic provinces, and oil and gas fields released by the U.S.G.S. World Energy Project obtained in vector shape (.shp).

4. The geoid gravitational model of Iran (Figure 4) is based on using the EGM-2008 grid (Pavlis et al., 2012) applied in studies on geophysics and geology (Lemenkova, 2020b).

5. The 3D relief model of Zagros mountains (Figure 5) is based on the ETOPO5 raster grid (Amante and Eakins, 2009). The ETOPO presents a numerical model data of the Earth's topography. Similar to GEBCO, it has a global coverage but with lower resolution, which is useful for plotting big data sets due to reduced computer processing time (e.g., GEBCO grid has an 11.72 Gb size for the global grid, while the 'earth_relief_05m.grd' has 10.8 Mb size, which fastens the 3D modelling). The 3D modelling and applications of ETOPO1 grids have been reported in previous works (Lemenkova, 2020f, 2021f; Spooner et al., 2020; Vérard et al., 2015), where their effectiveness is presented.

6. The free-air gravity anomaly (Figure 6) is based on the open source geophysical datasets (Sandwell et al., 2014; Sandwell and Smith, 1997) and represents the gravity after a free-air correction applied for the elevation at which a measurement is made (that is, the mean sea level). The gravity modelling has been presented in various publications (Lemenkova, 2020c) and (Djamour et al., 2010) with techniques of visualization and theoretical basis explained with reference to geology. The geophysical fieldwork often uses magnetic, gravimetric and deep crustal seismic (reflection and refraction/wide-angle) surveys, which provide the necessary database for detailed mapping (Lemenkova, 2021b,c,d), but this study is fully based on the computer-based data processing using shell scripting cartographic techniques for applied geology.

7. The five geomorphometric maps (Figure 7–11) are based on the DEM embedded in RStudio environment (RStudio Team, 2017) of R programming language (R Core Team, 2020) by library 'raster', which was called by the country name using the following code: 'alt = getData("alt", country = "Iran", path = tempdir())'. The dataset was then uploaded to the RStudio project and used for further processing: modelling slope, aspect, hillshade and terrain relief of Iran using libraries 'raster' (Hijmans and van Etten, 2012) and 'tmap' (Tennekes, 2018), which have their syntax along with common general syntax of R presented in geoscience publications (Lemenkova, 2019b).

3.1. Mapping by GMT

The maps in GMT are performed in several stages using several GMT modules (Wessel et al., 2019) using occasional data processing (converting, projection, retrieving data information) by GDAL (GDAL/OGR, 2021). The general steps are given as follows. Image capture and visualisation by the code 1:

```
gmt grdconvert n00e45/w001001.adf geoid_IR.grd
gmt grdconvert n00e00/w001001.adf geoid_IQ.grd
gdalinfo geoid_IR.grd -stats
gdalinfo geoid_IQ.grd -stats
gmt makecpt -Chaxby -T-100/50/1 > colors.cpt
% initiating the file
ps=Geoid_IR.ps
gmt grdimage geoid_IR.grd -Chaxby -R43/65/24/40 -JM6.5i
-P -I+a15+ne0.75 -Xc -K > $ps
gmt grdimage geoid_IQ.grd -Ccolors.cpt -R -J -P
-I+a15+ne0.75 -Xc -O -K >> $ps
```

Listing 1. GMT code for converting formats and visualising raster in Figure 4

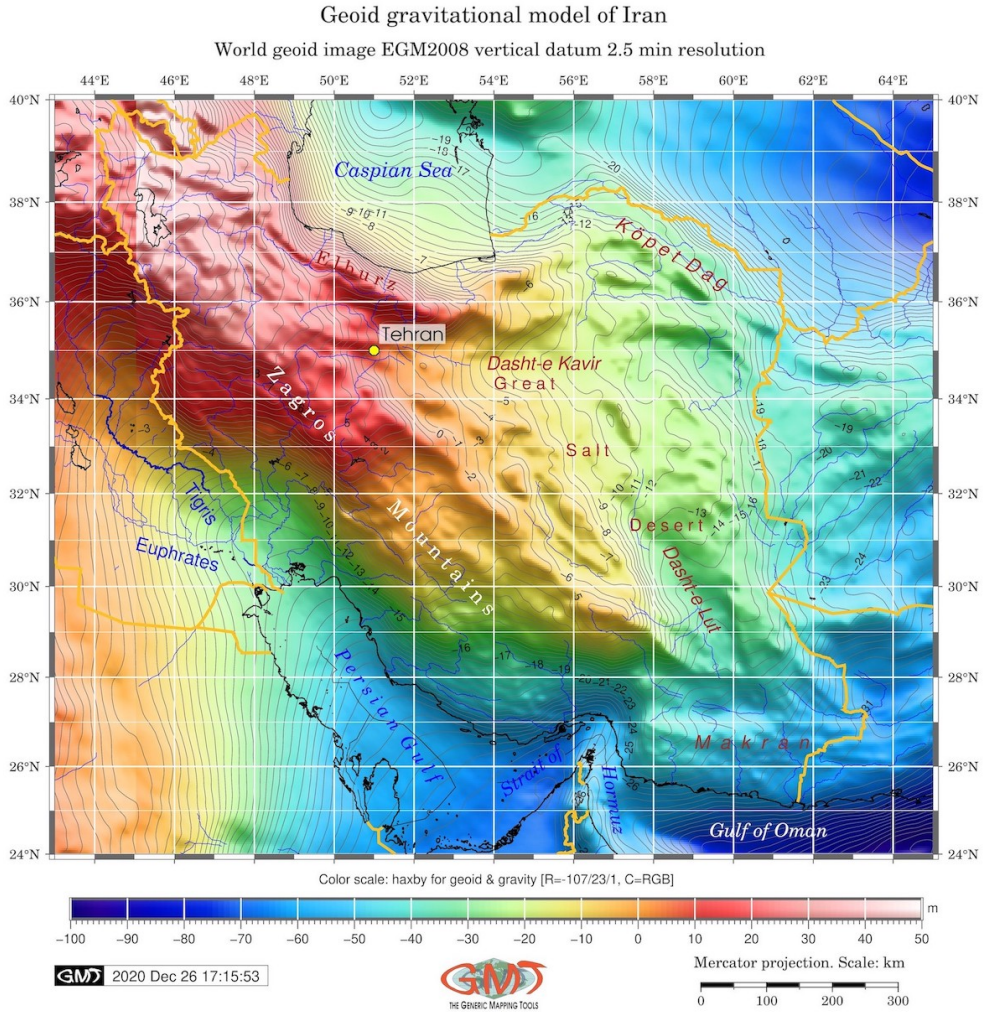

Figure 4. Geoid model of Iran. Data source: *Earth Gravitational Model (EGM-2008)*, Pavlis et al. (2012). Mapping in GMT.

The topographic image was uploaded to GMT and visualised using the coordinate extent by using the 'grdimage' module. Adding cartographic grid by the code 2 using the 'psbasemap' module of GMT:

```
gmt psbasemap -R -J -Bpxg2f1a2 -Bpyg2f1a2 -Bsxg2 -Bsyg1 \
    --MAP_TITLE_OFFSET=1.0c --MAP_ANNOT_OFFSET=0.1c \
    --FONT_TITLE=12p,25,black --FONT_ANNOT_PRIMARY=7p,25,black \
    --FONT_LABEL=8p,25,black --MAP_FRAME_AXES=WEsN -B+t"Geoid gravitational model of Iran" \
    -Lx14.0c/-2.5c+c318/-57+w300k+l"Mercator projection. Scale: km"+f -UBL/0p/-70p -O -K >> $ps
```

Listing 2. GMT code for plotting cartographic grid on the image

Text annotations are plotted using the code in 3 (abbreviated example with selected names), where the '56.7 26.0' in the line 3 signify the longitude/latitude coordinates of the location and the '+a-80' flag means the rotation of the text. Similar logic has been used throughout:

```
gmt pstext -R -J -N -O -K -F+jTL+f10p,26,blue1+jLB+a-80
>> $ps << EOF
56.7 26.0 Hormuz
EOF
gmt pstext -R -J -N -O -K \
-F+f10p,13,black+jLB -Gwhite@30 >> $ps << EOF
51.2 35.2 Tehran
EOF
gmt psxy -R -J -Sg -W0.5p -Gyellow -O -K << EOF >> $ps
51.0 35.0 0.20c
EOF
gmt pstext -R -J -N -O -K \
-F+f10p,13,black+jLB -Gwhite@30 >> $ps << EOF
51.2 32.2 Isfahan
EOF
gmt psxy -R -J -Sc -W0.5p -Gyellow -O -K << EOF >> $ps
51.0 32.0 0.15c
EOF
```

Listing 3. GMT code for plotting textual annotations on the image

The insert globe map was added on the main image using the code 4:

```
# Countries codes: ISO 3166-1 alpha-2.
gmt psbasemap -R -J -O -K -DjTR+w3.2c+o-0.2c/-0.2c+stmp >> $ps
read x0 y0 w h < tmp
gmt pscoast --MAP_GRID_PEN_PRIMARY=thin,grey -Rg -JG54/32N/$w -Da -Glightgoldenrod1 -A5000 -Bga \
-Wfaint -EIR+gred -Sdodgerblue -O -K -X$x0 -Y$y0 >> $ps
gmt psxy -R -J -O -K -T -X-${x0} -Y-${y0} >> $ps
```

Listing 4. GMT code for inserting a small globe map on the image in Figure 1.

Similar logic of the modular-based cartographic plotting was applied for maps in Figures 1, 2, 5 and 6. The PostScript files were converted into JPG format by 'psconvert' using the code 5:

```
gmt psconvert Topo_IR.ps -A0.2c -E720 -Tj -Z
```

Listing 5. GMT code visualizing the image

The 3D modelling in Figure 5 (3D model of Zagros) was performed using the code in Listing 6:

```
gmt grdcut earth_relief_05m.grd -R43/65/24/40 -Gir_relief.nc
gmt makecpt -Cturbo.cpt -V -T-3487/5149 > myocean.cpt
ps=IR3D165.ps
gmt grdcontour earth_relief_05m.grd -JM10c -R43/65/24/40 -p165/30 -C750 -B4/4NESW -Gd3c -Y3c \
    -U/-0.5c/-1c/"Data: World ETOPO 5 arc min grid" -P -K > $ps
gmt pstext -R -J -N -O -K \
-F+jTL+f9p,25,blue1+jLB+a-50 >> $ps << EOF
50.0 28.5 Persian Gulf
EOF
gmt pstext -R -J -N -O -K -F+jTL+f10p,25,brown+jLB+a-47 -Gwhite@30 >> $ps << EOF
52.0 30.5 Zagros Mts
EOF
gmt pscoast -R43/65/24/40 -J -p165/30 -P -Ia/thinner,blue -Na -W0.1p -Df -O -K >> $ps
gmt psscale -Dg37.5/24+w8.0c/0.4c+v+o0.0/0.5c+ml \
    -R -J -Cmyocean.cpt -Bg500f50a500+l"Color scale legend: depth and height elevations (m)." \
    -I0.2 -By+lm -O -K >> $ps
gmt grdview ir_relief.nc -J -R -JZ3c -Cmyocean.cpt -p165/30 -Qsm -N-3500+glightgray \
    -Wm0.07p -Wf0.1p,red -B4/4/2000:"Bathymetry and topography (m)":ESwZ -S5
    -Y5.0c -O -K >> $ps
gmt pstext -R -J -N -O -K -F+jTL+f9p,25,blue1+jLB+a-53 >> $ps << EOF
49.0 32.0 Persian Gulf
EOF
gmt pstext -R -J -N -O -K -F+jTL+f10p,25,white+jLB+a-47 >> $ps << EOF
48.0 36.5 Z a g r o s  M o u n t a i n s
EOF
gmt pstext -R -J -N -O -K -F+jTL+f9p,26,white+jLB >> $ps << EOF
59.7 25.0 Gulf of Oman
EOF
# Add GMT logo
gmt logo -Dx10.5/-5.5+o0.0c/-0.5c+w2c -O -K >> $ps
# Add title
gmt pstext -R0/10/0/10 -Jx1 -X-0.8c -Y0.0c -N -O -K -F+f10p,Helvetica,black+jLB >> $ps << EOF
0.0 8.2 Zagros Mountains: 3D topographic mesh model
0.0 7.7 Base map: 2D relief contour plot
0.0 7.2 Region: Iran
EOF
gmt pstext -R0/10/0/10 -Jx1 -X0.0c -Y0.0c -N -O -F+f8p,Helvetica,black+jLB >> $ps << EOF
7.0 7.0 Perspective view, azimuth rotation: 165/30\232
EOF
# Convert to image file by GhostScript
gmt psconvert IR3D165.ps -A1.2c -E720 -Tj -P -Z
```

Listing 6. GMT code for 3D image visualisation in Figure 5.

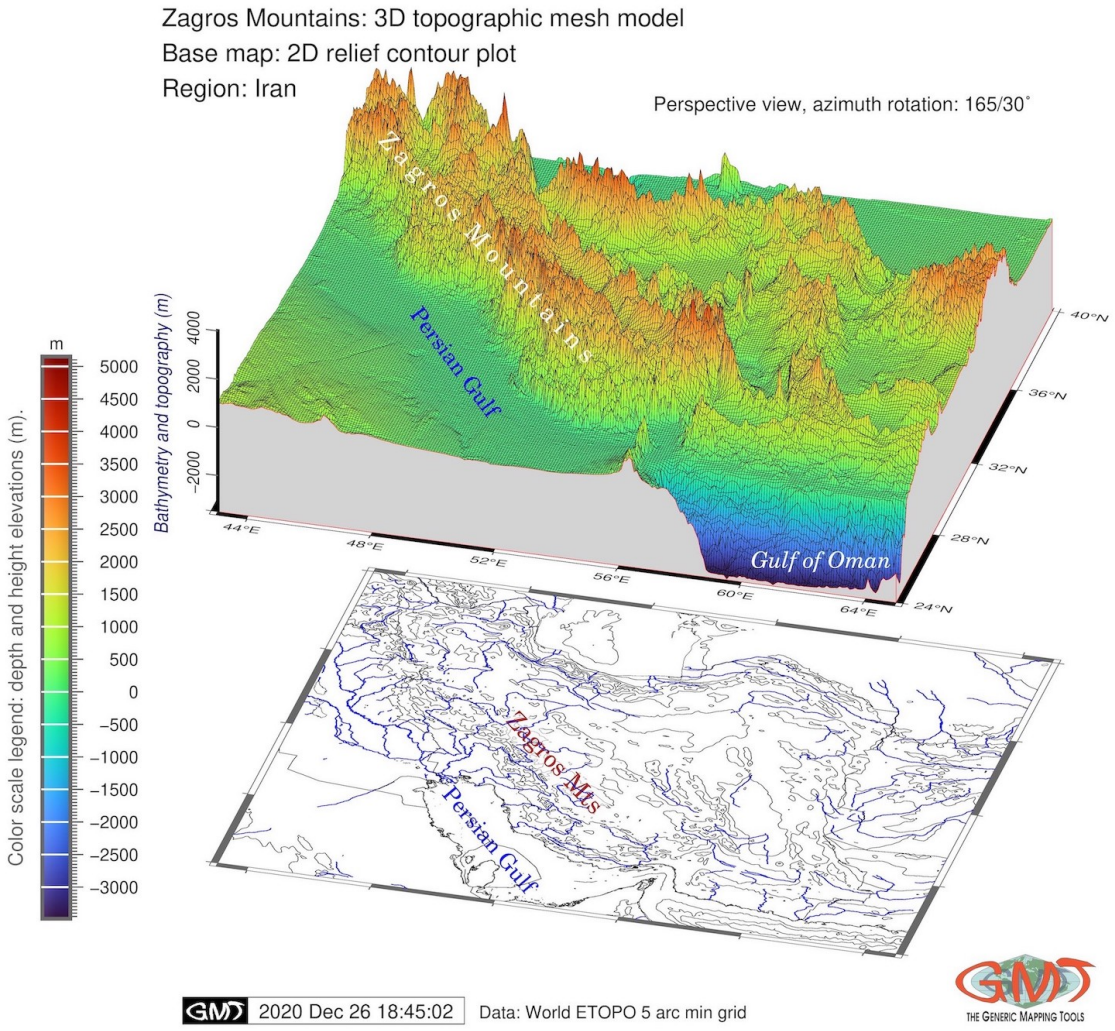

Figure 5. 3D model of Zagros mountains. Data source: *ETOPO 5-minute gridded elevation data*, Data Announcement 88-MGG-02, Digital relief of the surface of the Earth. NOAA, National Geophysical Data Center, Boulder, Colorado, U.S.A., 1988. URL: ETOPO5. Mapping in GMT.

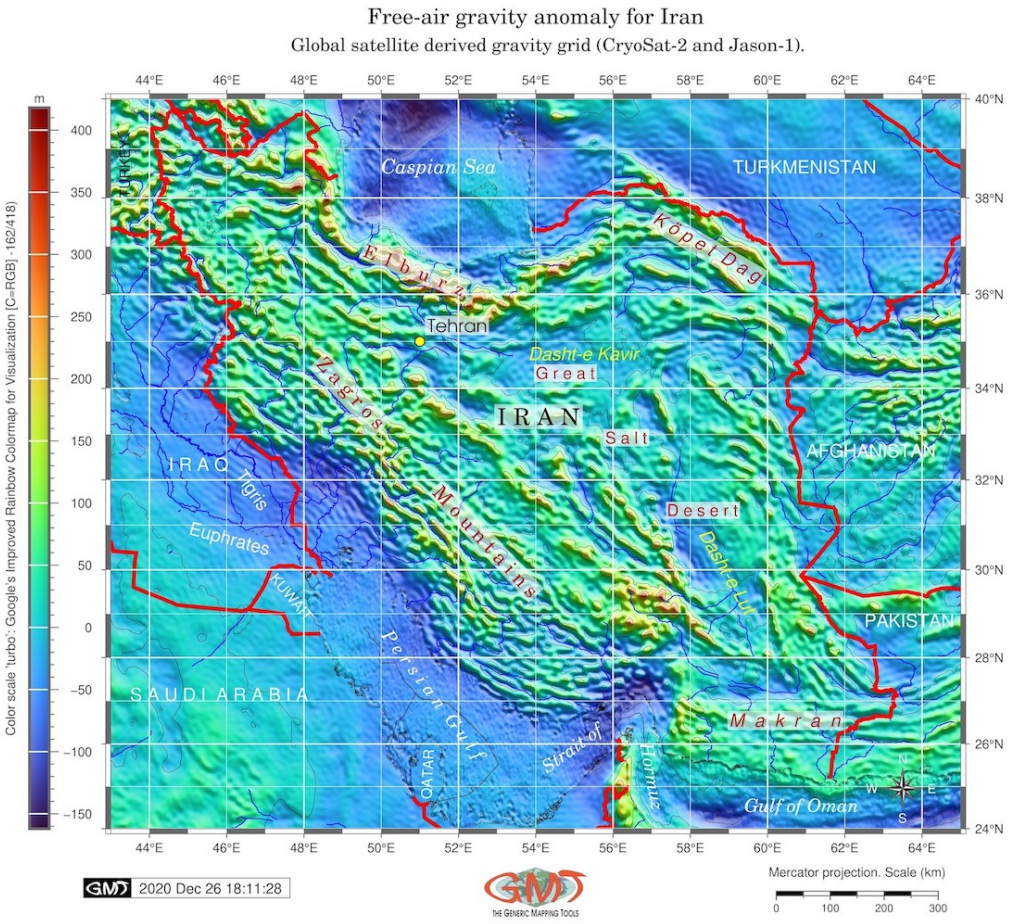

Figure 6. Free-air gravity anomaly of Iran. Data source: *gravity anomaly from Geosat and ERS 1 satellite altimetry*, Sandwell and Smith (1997). Mapping in GMT.

3.2. Cartographic visualization by QGIS

The cartographic visualization by QGIS was used for mapping Figures 2 and 3 showing geologic and lithologic maps of Iran visualizing its spatial variability and complexity of its structure. The maps were plotted using the general approach of Geographic Information Systems (GIS) by the graphical user interface (GUI), which contains a user menu well known and applied in traditional cartography, e.g., GIS and applied modelling in environmental studies (Klaučo et al., 2017, 2013), geologic and geophysical modelling (Lindh and Lemenkova, 2021b, 2022b).

3.3. Plotting by R language

The maps in Figures 7–11 are plotted using R language in RStudio integrated development environment, which combines a console for coding and a graphical menu for visualisation of plots. The main approach by 'raster' package of R consists in visualising geomorphometric models using DEM. The data were captured using the following code 7:

```
library(sp)
library(raster)
library(ncdf4)
library(RColorBrewer)
library(sf)
library(tmap)
alt = getData("alt", country = "Iran", path = tempdir())
```

Listing 7. R code for data capture and uploading necessary packages

To extract the relief characteristics of the Iranian Plate, the 'raster' package of R was used. The results were visualized as several thematic maps Figures 7 to 11 presenting a series of morphometric analyses, modelled in 'raster' package with a default visualisation and then adjusted in 'tmap' package for a better cartographic setting: 1) slope analysis, Figures 7 and 8; 2) aspect maps, Figure 9; 3) hill shade map, Figure 10; 4) DEM elevation map, Figure 11.

The 'raster' package has a straightforward syntax and rather simplified manner of cartographic data processing. The code for modelling is as follows: slope = terrain(alt, opt = "slope"), where the 'opt' function was changed for 'aspect' and 'alt' aimed to visualize aspect and elevation. The hillshade was visualised using the theoretical terrain computations described in Horn (1981). The value of hillshade modelling consists in mapping the surface topography, which includes visual depth cue. The visualisation is theoretically based on the dependence of the elevation depicted on a map on the tone of gray or colour level, as well as the compass orientation of the topographic surface elements. The hillshade was visualised by the code 8:

```
slope = terrain(alt, opt = "slope")
plot(slope)
aspect = terrain(alt, opt = "aspect")
plot(aspect)
hill = hillShade(slope, aspect, angle = 40,
direction = 270)
plot(hill)
plot(alt)
tmap_save(alt, "Iran_Slope.jpg", dpi = 300, height = 10)
```

Listing 8. R code visualizing the geomorphological parameters and saving the output data

The example of the code for cartographic adjustments is as follows, Listing 9:

```
# tmaptools::palette_explorer()
tmap_mode("plot")
map1 <-
    tmap_style("watercolor") +
    tm_shape(slope, name = "Slope", title = "Slope") +
    tm_raster(
        title = "Slope (0\u00B0-90\u00B0)", palette = "-Set1", style = "quantile", n = 10,
        breaks = c(5, 10, 20, 30, 40, 50, 60, 70, 80, 90), legend.show = T,
        legend.hist = T, legend.hist.z=0) +
    tm_scale_bar(
        width = 0.25, text.size = 0.8, text.color = "black",
        color.dark = "black",color.light = "white", position=c("center", "bottom"), lwd = 1) +
    tm_compass(
        type = "radar", position=c("right", "top"), size = 10.0) +
    tm_layout(scale = .8,
        main.title = "Slope terrain analysis <...> R", main.title.position = "center",
        main.title.color = "black", main.title.size = 1.0,
        title = "Slope (0\u00B0-90\u00B0)", title.color = "black",
        title.size = 1.0, title.position = c("left", "top"),
        panel.labels = c("R: tmap, raster, sp, sf"), panel.label.color = "darkslateblue",
        panel.label.size = 1.0, legend.position = c("left","bottom"),
        legend.bg.color = "grey90", legend.bg.alpha = .2,legend.outside = FALSE,
        legend.width = .3, legend.height = .5, legend.hist.height = .2,legend.title.size = 0.9,
        legend.text.size = 0.8, inner.margins = 0) +
    tm_graticules(
        ticks = TRUE,  lines = TRUE, labels.rot = c(15, 15),
        col = "azure3", lwd = 1, labels.size = 1.0)
# plot map
map1
tmap_save(map1, "Iran_Slope.jpg", dpi = 300, height = 10)
```

Listing 9. R code for visualisation of the geographic map in Figure 8.

The default visualization of the ‘raster’ package is illustrated in Figure 7, which shows a slope map of Iran. After the initial models were created, the data for each map in Figures 8–11 were imported to the ‘tmap’ package where cartographic processing is more sophisticated. For instance, the cartographic elements are adjusted using special flags in the options of the function.

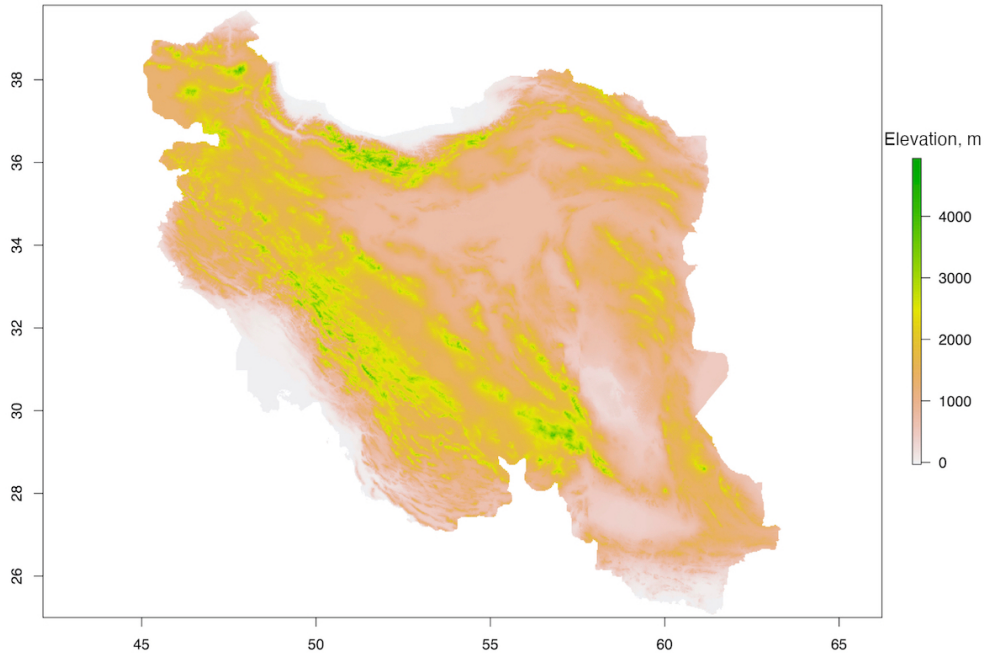

Figure 7. Elevation model by R ‘raster’ package. Data source: *Shuttle Radar Topography Mission (SRTM) DEM*, Farr and Kobrick (2000). Mapping in R.

The ’tmap’ functions ’tm_scale_bar’, ’tm_raster’ and ’tm_graticules’ were used for plotting self-explaining cartographic elements. The main adjustments of the graphical output were set up in the ’tm_layout’ function where the following elements were visualized (colour, size, locations of the elements on the map): legend, panel annotations, title and labels.

The relationship between the geomorphological elements, such as slope, aspect, elevation (Figures 8–11), 3D topographic model (Figure 5), lithologic and geologic structure of Iran (Figures 2 and 3) was used to analyse the variations of the homogeneity of the relief, i.e., if the area has an increasingly higher variations in slope and steepness in Zagros Mountains or the dominating landforms are the stable low-level lowlands mostly located in the basin of tributaries of Tigris River in the south-western part of Iran. Then the histograms for each of the morphometric maps were created using the ’legend.hist = T’ option in the ’tm_raster’ function based on the automatically analysed data distribution.

4. RESULTS AND DISCUSSION

The comparisons of the topographic, geological, geomorphological and geophysical maps as well as the values of general morphometric elements (slope, aspect, hillshade and elevation) with the relief map revealed that the regions of the Zagros fold and thrust zones often corresponds to differing morphometric properties. For instance, higher values of Elburz and Zagros ranges, selected ranges of Kopet Dag and Makran slopes (Figure 1) shown as bright red colours in Figure 8 are associated with the extreme steep slopes, while major deserts of Iran, such as Dasht-e Kavir, Dasht-e Lut and Great Salt Desert (Figure 1), are mostly associated with the slopes having the lowest steepness (grey colours in Figure 8).

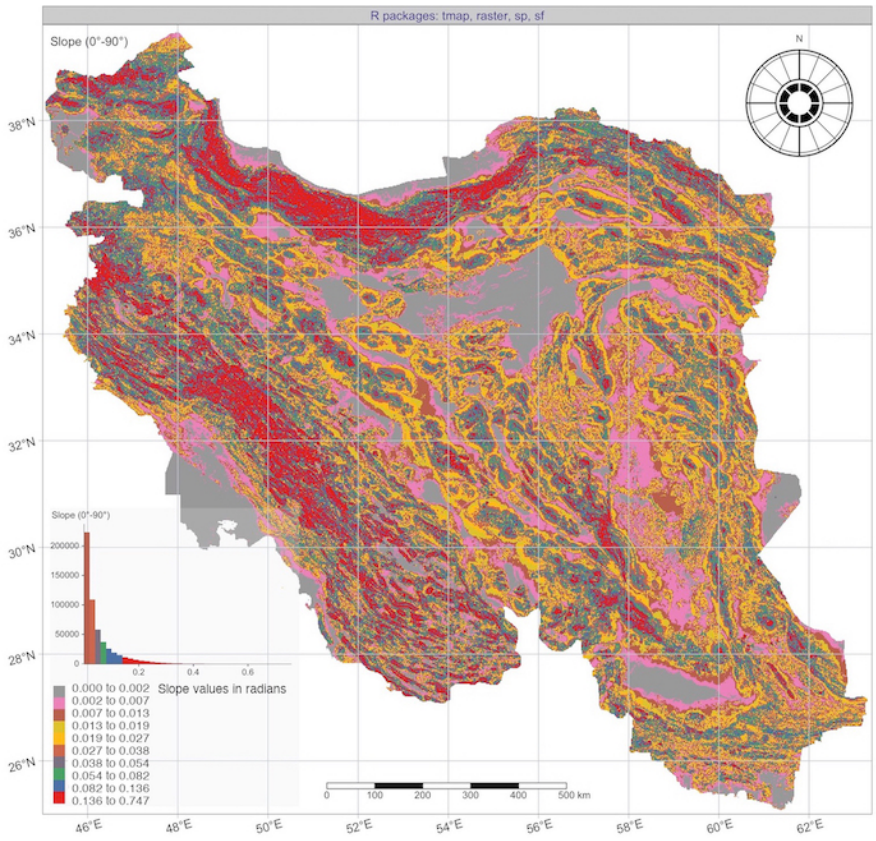

Figure 8. Slope terrain model based on DEM of Iran. Data source: *Shuttle Radar Topography Mission (SRTM) DEM*, Farr and Kobrick (2000). Mapping in R.

Three distinct Fold Belts shown in Figure 3 – the Kopet Dag, Elburz and Zagros – have the dense locality of major faults (shown red in Figure 3) that are associated with the geologic formation controlled by the tectonic constraints on the evolution (e.g., salt-bearing Neogene sediments are folded and cut by faults in Alborz Mountains), as it is also reported in the existing works (Baikpour et al., 2010; Burberry et al., 2010). Variations in the fold patterns, geologic characteristics and deformation style can be seen by comparison of the Figures 2 and 4 showing the three-dimensional and plain map visualizations of topography and geology.

The variations in the relief changing according to various areas of Zagros belt are also reported in previous publications (Casciello et al., 2009; Hessami et al., 2001; Jiménez-Munt et al., 2012). The geologic structure of Zagros Fold-and-Thrust Belt, including visualized geologic provinces, major faults, surficial lithologic boundaries and bedrock geology also affects both the local shape of geomorphic landforms of Iran and the slope steepness.

The geophysical discontinuities (Figure 5)) and free-air gravity anomalies (Figure 6) were demonstrated by the two GMT-based maps showing a general increase of the geoid undulation values in southeast–northwest direction. That is, the Indian geopotential low-level geoid anomalies can be clearly seen (Figure 5) as low values (below 60 m, coloured blue to deep blue in Figure 5 while Zagros fol and thrust belt are mostly covered by the slightly positive values (above minus 10 to 5: yellow to orange colours in south-east Zagros area), followed by the strongly positive values of above 5 m (bright red colours in Figure 5), which shows an increase of the geoid heights along the Zagros mountains chain.

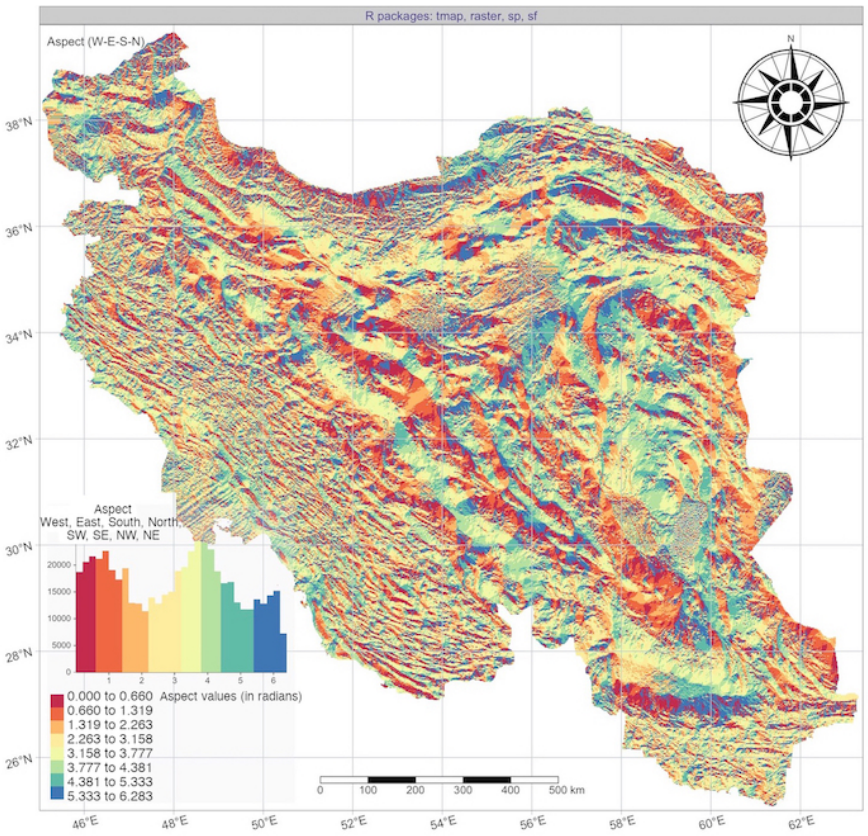

Figure 9. Aspect terrain model of Iran. Data source: *Shuttle Radar Topography Mission (SRTM) DEM*, Farr and Kobrick (2000). Mapping in R.

The basin of Persian Gulf demonstrates mostly negative values from minus 65 to minus 40 m (light blue colours in Figure 5) with slightly negative values in the Tigris and Euphrates rivers (aquamarine colours, from minus 40 to minus 20 m). The general geophysical properties, such as free-air gravity (Figure 6), also correspond to the geologic rock types and lithology of the region. This can be seen by the comparison of Figures 3 and 6 where isolines of gravity correspond to the lithological rock types distribution, which points to the strong correlation between the geophysical and geological setting due to the rock density, porosity and structure.

The geomorphometry of Iran in general and the Zagros mountain in particular, as its most remarkable landform and relief feature (e.g., Elburz, Kopet Dag mountain chains) is visualized in the set of figures plotted in R. The specifics of the Elburz Mountains includes alluvial fans, which are particularly well developed along their southern margins, as also noted in previous studies (Beaumont, 1972) The evaluation of slope (Figures 7 and 8), aspect orientation of slopes (Figure 9), hillshade with artificial illumination highlighting the relief (Figure 10) and DEM-based visualization of the geomorphological properties better highlight the geologic structure of Zagros and the surrounding relief (Figure 11). These models were plotted to show complex landforms along the Zagros Fold-and-Thrust Belt and in other regions of country.

The wide river valleys (e.g., tributaries of the Tigris River) have a gentler, almost flat relief with low-leveled, smoothed and gentle slopes. On the contrary, mountainous areas have steeper slope gradients, suggesting that the geologic evolution of the Zagros Fold-and-Thrust Belt formation created a complex alteration between the large and gentle landforms. At the same time, local development of the flattened relief in the Dasht-e Kavir, Dasht-e Lut and Great Salt Desert is evident by the comparative analysis between the maps in Figure 1 with Figures 7 and 8 (slope), as well as Figure 9 (aspect), with Figures 10 and 11 (relief).

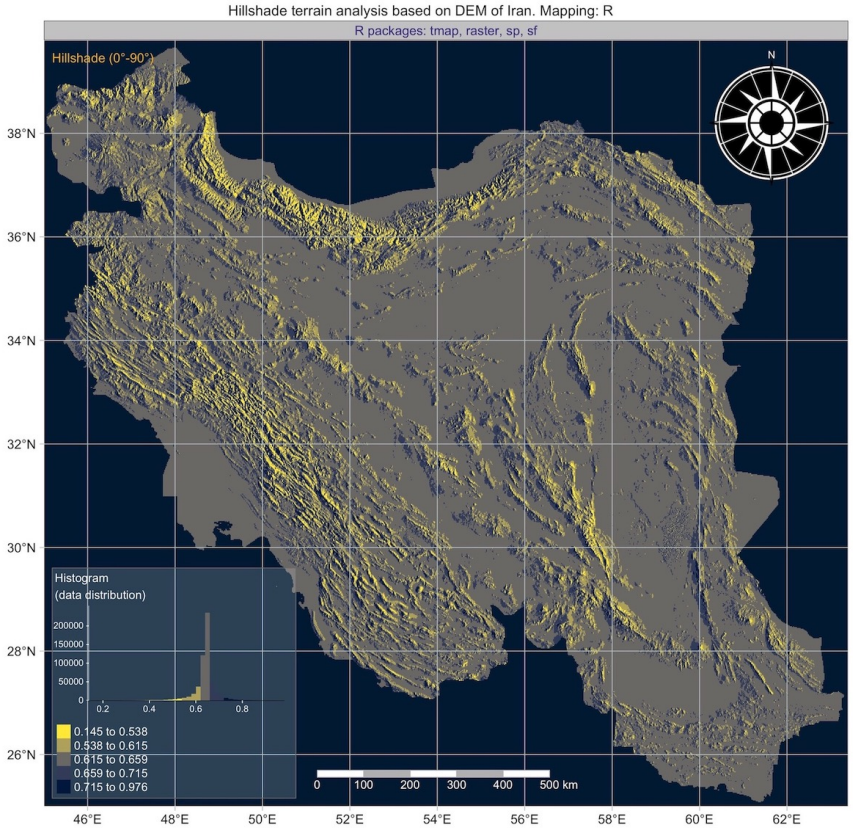

Figure 10. Hillshade terrain model of Iran. Data source: *Shuttle Radar Topography Mission (SRTM) DEM*, Farr and Kobrick (2000). Mapping in R.

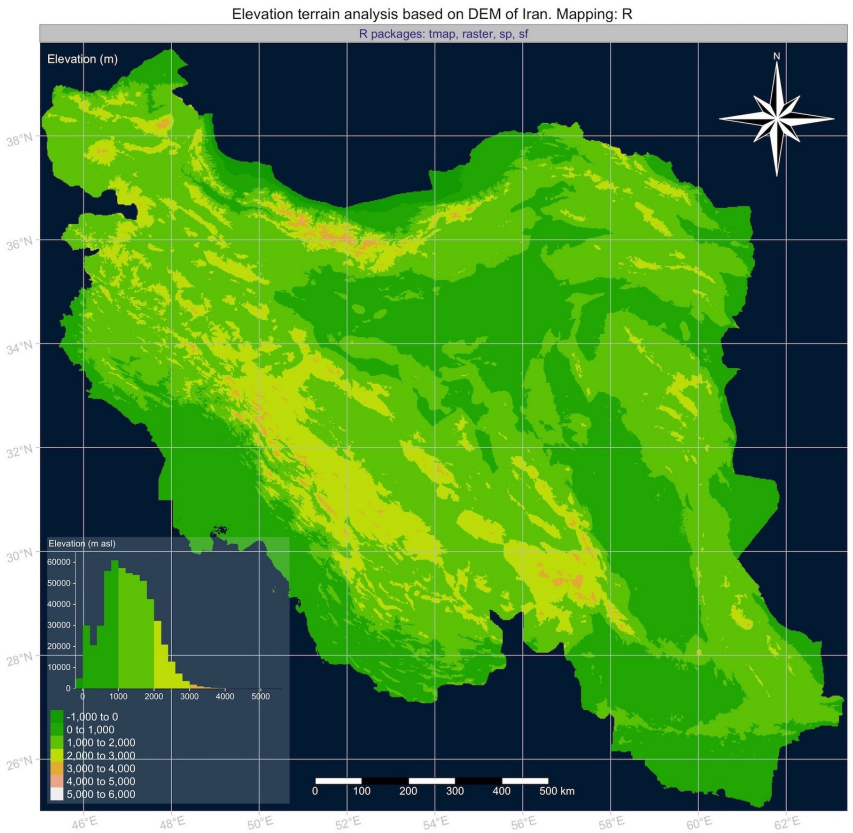

Figure 11. DEM elevation model of Iran. Data source: *Shuttle Radar Topography Mission (SRTM) DEM*, Farr and Kobrick (2000). Mapping in R.

5. CONCLUSIONS

This paper addressed the issues of cartographic data processing and visualization using scripts and traditional GIS. Specifically, the use of QGIS and GMT was presented and proposed an efficient scheme of 2D and 3D modelling of the multi-source spatial data. Different from traditional GIS, the GMT can not only process geospatial data in an accurate and rapid way effectively, but also enables advanced 3D modelling. The performance and functionality of both GMT and QGIS were evaluated comprehensively on 11 datasets used for plotting a series of maps. Moreover, the geologic analysis and the comparison of maps were performed using new maps and the available literature.

This study presented a script-based mapping of the geomorphology of Zagros Fold-and-Thrust Belt using a combination of GMT, R and QGIS tools for 2D and 3D modelling. The 2D and 3D visualization of geomorphology of Zagros Basin, together with mapping of the geophysical fields, helped to analyse the tectonic-geologic structure of this region formed under the strong influence of complex interaction between the Arabian and Eurasian tectonic plates. The integrated use of GIS and GMT presented a well-balanced combination of technical cartographic tools for 2D and 3D visualization of the topographic, geological and geophysical data.

The actuality and technical novelty of this research consists in the scripting used for mapping. Besides, the integration of several tools was applied for interpretation of the geomorphology of Iran, which is largely affected by geophysical and geodynamic setting. This study is based on using multi-source data from the open source datasets: topographic (GEBCO/SRTM, ETOPO), geophysical (Faye's gravity, geoid EGM-2008), geological and tectonic mapping, 2D and 3D data models, lithological maps from the UNESCO datasets and DEM embedded in R library 'raster'. The data were integrated to construct a regional project on the Iranian geomorphology and to develop a series of maps covering Zagros area and the surroundings. The integration of the high-resolution datasets resulted in the 11 new maps presented in this study. Moreover, the study was supported and complemented by the extended analysis of the literature resources on the Zagros Fold-and-Thrust Belt and the geomorphology of the Iranian Plate.

The presented multi-source thematic geodata modelling helped to describe the geomorphic variations in Zagros Fold-and-Thrust Belt and assist in the monitoring of its mineral resources. The main results define the significant geomorphological variations along the Zagros mountains belt and within Iran. In addition, using the geomorphometric analysis by means of R language, this paper provided a numerical evaluation and visual presentation of the slope, aspect and hillshade relief visualization illustrating the topographic structure of the Zagros basin.

Using scripting technical approach by a combination of GMT and R supported by the GIS mapping in QGIS, the multi-source datasets combined from the open data sources on Iran have been compiled and visualized in conjunction with new tools of cartographic data analysis with the aim of providing new interpretations of the geomorphology, geology and topography of Iran. Thus, this paper provides a better cartographic picture of the geologic structures, geophysical anomaly fields, 2D and 3D models and tectonic deformation lineaments of Iran with a particular focus on Zagros mountains as a major geomorphological structure of the country. Besides Zagros mountains, the Elburz and Kopet Dag belts were visualized and analysed together with Dasht-e Kavir, Dasht-e Lut and Great Salt Desert as the significants geomorphological structures of Iran.

These geomorphological zones were analysed by means of R geomorphometric analysis and quantitative maps were presented for the slope and aspect maps showing histograms of data frequency for each class of the slope steepness and aspect orientation by the compass direction (major West, East, South and North and the derivative ones), which divide the country into the

zones with different geomorphological and topographic patterns well correlating with geophysical setting, and geological and lithological structure. These variations mirror different geological structural characteristics developing along the Zagros Fold-and-Thrust Belt during the tectonic plate collision (Arabian and Eurasian) as a result of the geologic evolution (Schoenbohm, 2022).

The automation in cartographic analysis has been the point of discussion in various papers (Ebi, 1995; Gilliot et al., 1993; Kazemi et al., 2005; Lemenkova, 2019a, 2022c,d,e; Lopez-Ornelas and Sedes, 2008) and widely used recently along with rapid progress of the machine learning and development of the scripting languages. The presented integrated combination of various scripting mapping tools in one project, as demonstrated in this paper, has shown the effectiveness of the computer-based methods in cartographic workflow with a case of the geomorphology of Iran with a special focus on Zagros Fold-and-Thrust Belt. Thus, this study hybridizes the traditional mapping presented by the QGIS and the scripting cartographic method of GMT and two special packages of R ('raster' and 'tmap') used to visualze 2D and 3D topographic, geophysical and geological maps of Iran.

The importance of the Zagros Fold-and-Thrust Belt as a study area is explained by its unique geologic and geomorphological structure, which contains vast mineral resources of Iran (Motaghi, Shabanian and Kalvandi, 2017; Regard et al., 2004; Saura et al., 2015; Sepehr and Cosgrove, 2004). At the same time, this region is subject to seismic activity and earthquakes, as reported in various papers (Nissen et al., 2011; Paul et al., 2006; Talebian and Jackson, 2004; Tavakoli et al., 2008; Yamini-Fard et al., 2006). Besides, the Zagros mountain chain significantly influences the surrounding nature, environmental and climate conditions of Iran as a major distinct topographic landmark of the country controlling the habitats, vegetation and landscape distribution, and serving as a key geomorphological structure of Iran.

Acknowledgements. The author would like to thank the editors and the two anonymous reviewers for careful reading the manuscript, constructive comments and suggestions that improved both the text and the maps.

REFERENCES

Adams, A., Brazier, R., Nyblade, A., Rodgers, A. and AlAmri, A. (2009). Source parameters for moderate earthquakes in the Zagros mountains with implications for the depth extent of seismicity, *Bulletin of the Seismological Society of America* **99**: 2044–2049. https://doi.org/10.1785/0120080314.

Afzal, P., Heidari, S. M., Ghaderi, M. and Yasrebi, A. B. (2017). Determination of mineralization stages using correlation between geochemical fractal modeling and geological data in Arabshah sedimentary rock-hosted epithermal gold deposit, NW Iran, *Ore Geology Reviews* **91**: 278–295.

Ahmadhadi, F., Daniel, J., Azzizadeh, M. and Lacombe, O. (2008). Evidence for pre-folding vein development in the Oligo-Miocene Asmari Formation in the Central Zagros Fold Belt, Iran, *Tectonics* **27**: TC1016. https://doi.org/10.1029/2006TC001978.

Alavi, M. (1994). Tectonics of the Zagros orogenic belt of Iran: new data and interpretations, *Tectonophysics* **229**: 211–238. https://doi.org/10.1016/0040-1951(94)90030-2.

Alavi, M. (2004). Regional stratigraphy of the Zagros fold-thrust belt of Iran and its pro- foreland evolution, *American Journal of Science* **304**: 1–20. https://doi.org/10.2475/ajs.304.1.1.

Alavi, M. (2007). Structures of the Zagros fold-thrust belt in Iran, *American Journal of Science* **307**: 1064–1095. https://doi.org/10.2475/09.2007.02.

Ali, S. A., Buckman, S., Aswad, K. J., Jones, B. G., Ismail, S. A. and Nutman, A. P. (2012). Recognition of late cretaceous hasanbag ophiolite-arc rocks in the Kurdistan region of the Iraqi zagros suture zone: a missing link in the paleogeography of the closing Neotethys ocean, *Lithosphere* **4**: 395–410. https://doi.org/10.1130/L207.1.

Ali, S. A., Mohajjel, M., Aswad, K., Ismail, S., Buckman, S. and Jones, B. (2014). Tectono-stratigraphy and general structure of the northwestern Zagros collision zone across the Iraq-Iran border, *Environmental Earth Sciences* **4**: 92–110.

Allen, M. B., Saville, C., Blanc, E. J., Talebian, M. and Nissen, E. (2013). Orogenic plateau growth: Expansion of the Turkish-Iranian Plateau across the Zagros fold-and-thrust belt, *Tectonics* **32**: 171–190. https://doi.org/10.1002/tect.20025.

Amante, C. and Eakins, B. W. (2009). Etopo1 1 arc-minute global relief model: Procedures, data sources and analysis, NOAA Technical Memorandum, 19. https://www.ngdc.noaa.gov/mgg/global/relief/ETOPO1/docs/ETOPO1.pdf.

Andreo, V., Dogliotti, A. I., Tauro, C. and Neteler, M. (2015). Spatio-temporal variations in chlorophyll-a concentration in the patagonic continental shelf: An example of satellite time series processing with GRASS GIS temporal modules, *2015 IEEE International Geoscience and Remote Sensing Symposium (IGARSS)*, pp. 2249–2252.

Aubourg, C., Smith, B., Bakhtari, H. R., Guya, N. and Eshraghi, A. (2008). Tertiary block rotations in the Fars Arc (Zagros, Iran), *Geophysical Journal International* **173**: 659–673.

Authemayou, C., Chardon, D., Bellier, O., Malekzadeh, Z., Shabanian, E. and Abbassi, M. R. (2006). Late Cenozoic partitioning of oblique plate convergence in the Zagros fold-and-thrust belt (Iran), *Tectonics* **25**: TC3002. https://doi.org/10.1029/2005TC001860.

Bahroudi, A. and Koyi, H. A. (2003). Effect of spatial distribution of Hormuz salt on deformation style in the Zagros fold and thrust belt: an analogue modelling approach, *Journal of the Geological Society* **160**: 719–733. https://doi.org/10.1144/0016-764902-135.

Baikpour, S., Zulauf, G., Sebti, A., Kheirolahi, H. and Dietl, C. (2010). Analogue and geophysical modelling of the Garmsar Salt Nappe, Iran: constraints on the evolution of the Alborz Mountains, *Geophysical Journal International* **182**: 599–612. https://doi.org/10.1111/j.1365-246X.2010.04656.x.

Bayer, R., Chery, J., Tatar, M., Vernant, P., Abbassi, M., Masson, F., Nilforoushan, F., Doerflinger, E., Regard, V. and Bellier, O. (2006). Active deformation in Zagros–Makran transition zone inferred from GPS measurements, *Geophysical Journal International* **165**: 373–381. https://doi.org/10.1111/j.1365-246X.2006.02879.x.

Beaumont, P. (1972). Alluvial fans along the foothills of the Elburz Mountains, Iran, *Palaeogeography, Palaeoclimatology, Palaeoecology* **12**(4): 251–273.

Berberian, M. (1995). Master "blind" thrust faults hidden under the Zagros folds: active basement tectonics and surface morphotectonics, *Tectonophysics* **241**: 193–224. https://doi.org/10.1016/0040-1951(94)00185-C.

Beydoun, Z. R., Hughes, M. W. and Stoneley, R. (1992). Petroleum in the zagros basin: a late tertiary foreland basin overprinted onto the outer edge of a vast hydrocarbon-rich paleozoic-mesozoic passive-margin shelf, *in* R. W. Macqueen and D. A. Leckie (eds), *Foreland Basins and Fold Belts*, Vol. 55, AAPG Memoir, pp. 309–340. https://doi.org/10.1306/M55563C12.

Blanc, E. P., Allen, M. B., Inger, S. and Hassani, H. (2003). Structural styles in

the Zagros simple folded zone, Iran, *Journal of the Geological Society* **160**: 401–412. https://doi.org/10.1144/0016-764902-110.

Bosold, A., Schwarzhans, W., Julapour, A., Ashrafzadeh, A. R. and Ehsani, S. M. (2005). The structural geology of the High Central Zagros revisited (Iran), *Petroleum Geoscience* **11**: 225–238. https://doi.org/10.1144/1354-079304-646.

Burberry, C. M., Cosgrove, J. W. and Liu, J. G. (2010). A study of fold characteristics and deformation style using the evolution of the land surface: Zagros Simply Folded Belt. Iran, *Geological Society, London Special Publications* **330**: 139–154. https://doi.org/10.1144/SP330.8.

Casciello, E., Vergés, J., Saura, E., Casini, G., Fernández, N., Blanc, E., Homke, S. and Hunt, D. W. (2009). Fold patterns and multilayer rheology of the Lurestan Province, Zagros simply folded belt (Iran), *Journal of the Geological Society* **166**: 947–959. https://doi.org/10.1144/0016-76492008-138.

Cooper, M. (2007). Structural style and hydrocarbon prospectivity in fold and thrust belts: a global review, *in* A. C. Ries, R. W. Butler and R. H. Graham (eds), *Deformation of the Continental Crust: The Legacy of Mike Coward. Special Publications*, Vol. 272, London: Geological Society, London: UK, pp. 447–472. https://doi.org/10.1144/GSL.SP.2007.272.01.23.

De Sarkar, A., Biyahut, N., Kritika, S. and Singh, N. (2012). An environment monitoring interface using grass gis and python, *2012 Third International Conference on Emerging Applications of Information Technology*, pp. 235–238.

Djamour, Y., Vernant, P., Bayer, R., Nankali, H. R., Ritz, J., Hinderer, J., Hatam, Y., Luck, B., Le Moigne, N., Sedighi, M. and Khorrami, F. (2010). GPS and gravity constraints on continental deformation in the Alborz mountain range, Iran, *Geophysical Journal International* **183**: 1287–1301. https://doi.org/10.1111/j.1365-246X.2010.04811.x.

Ebi, N. B. (1995). Image interpretation of topographic maps on a medium scale via frame-based modelling, *Proceedings, International Conference on Image Processing*, Vol. 1, pp. 250–253.

Elyasi, S. (2016). Petroleum source-rock potential of the Piranj oil field, Zagros basin, *Marine and Petroleum Geology* pp. 448–454.

Eskandari, S. and Ali Mahmoudi Sarab, S. (2022). Mapping land cover and forest density in Zagros forests of Khuzestan province in Iran: A study based on Sentinel-2, Google Earth and field data, *Ecological Informatics* **70**: 101727.

Farr, T. G. and Kobrick, M. (2000). Shuttle radar topography mission produces a wealth of data, *Eos, Transactions American Geophysical Union* **81**(48): 583–585.

Garajeh, M. K., Feizizadeh, B., Blaschke, T. and Lakes, T. (2022). Detecting and mapping karst landforms using object-based image analysis: Case study: Takht-soleiman and parava mountains, iran, *The Egyptian Journal of Remote Sensing and Space Science* **25**(2): 473–489.

GDAL/OGR (2021). Geospatial data abstraction software library, https://gdal.org. Open Source Geospatial Foundation.

GEBCO Compilation Group (2020). Gebco 2020 grid, Dataset. https://doi.org/10.5285/a29c5465-b138-234d-e053-6c86abc040b9.

Gedicke, S., Bonerath, A., Niedermann, B. and Haunert, J.-H. (2021). Zoomless Maps: External Labeling Methods for the Interactive Exploration of Dense Point Sets at a Fixed Map Scale, *IEEE Transactions on Visualization and Computer Graphics* **27**(2): 1247–1256.

Gilliot, J.-M., Stamon, G. and Le Men, H. (1993). A knowledge-based system in image

processing for communication networks study in aerial images a tool for cartography automation, *Proceedings of IEEE Systems Man and Cybernetics Conference - SMC*, Vol. 2, pp. 77–82.

Heidari, S. M., Afzal, P., Ghaderi, M. and Sadeghi, B. (2021). Detection of mineralization stages using zonality and multifractal modeling based on geological and geochemical data in the Au-(Cu) intrusion-related Gouzal-Bolagh deposit, NW Iran, *Ore Geology Reviews* **139**: 104561.

Hessami, K., Koyi, H. A., Talbot, C. J., Tabasi, H. and E., S. (2001). Progressive unconformities within an evolving foreland fold—thrust belt, Zagros Mountains, *Journal of the Geological Society* **158**: 969–981. https://doi.org/10.1144/0016-764901-007.

Hijmans, R. J. and van Etten, J. (2012). raster: Geographic analysis and modeling with raster data, http://CRAN.R-project.org/package=raster. R package version 2.0-12.

Horn, B. (1981). Hill shading and the reflectance map, *Proceedings of the IEEE* **69**(1): 14–47.

Hosseini, S. T., Asghari, O. and Emery, X. (2021). An enhanced direct sampling (DS) approach to model the geological domain with locally varying proportions: Application to Golgohar iron ore mine, Iran, *Ore Geology Reviews* **139**: 104452.

Hrovat, A., Vilhar, A., Ozimek, I., Javornik, T. and Kočan, E. (2013). Grass-raplat - radio planning tool for grass gis system, *ICECom 2013*, pp. 1–5.

Huang, F., Liu, D., Liu, P., Wang, S., Zeng, Y., Li, G., Yu, W., Wang, J., Zhao, L. and Pang, L. (2007). Research on cluster-based parallel gis with the example of parallelization on grass gis, *Sixth International Conference on Grid and Cooperative Computing (GCC 2007)*, pp. 642–649.

Jahani, S., Callot, J., Letouzey, J. and Frizon de Lamotte, D. (2009). The eastern termination of the Zagros Fold-and-Thrust Belt, Iran: Structures, evolution, and relationships between salt plugs, folding, and faulting, *Tectonics* **28**: 1–22. https://doi.org/10.1029/2008TC002418.

Jiménez-Munt, I., Fernàndez, M., Saura, E., Vergés, J. and Garcia-Castellanos, D. (2012). 3-D lithospheric structure and regional/residual Bouguer anomalies in the Arabia–Eurasia collision (Iran), *Geophysical Journal International* **190**: 1311–1324. https://doi.org/10.1111/j.1365-246X.2012.05580.x.

Kasalica, V. and Lamprecht, A.-L. (2018). Automated composition of scientific workflows: A case study on geographic data manipulation, *2018 IEEE 14th International Conference on e-Science (e-Science)*, pp. 362–363.

Kazemi, S., Lim, S. and Ge, L. (2005). Integration of cartographic knowledge with generalization algorithms, *Proceedings. 2005 IEEE International Geoscience and Remote Sensing Symposium, 2005. IGARSS '05.*, Vol. 5, pp. 3502–3505.

Khodabakhshnezhad, A. and Arian, M. (2016). Salt Tectonics in the Southern Iran, *International Journal of Geosciences* **7**: 367–377. https://doi.org/10.4236/ijg.2016.73029.

Klaučo, M., Gregorová, B., Koleda, P., Stankov, U., Marković, V. and Lemenkova, P. (2017). Land Planning as a Support for Sustainable Development Based on Tourism: A Case Study of Slovak Rural Region, *Environmental Engineering and Management Journal* **16**(2): 449–458. https://doi.org/10.30638/eemj.2017.045.

Klaučo, M., Gregorová, B., Stankov, U., Marković, V. and Lemenkova, P. (2013). Determination of ecological significance based on geostatistical assessment: a case study from the Slovak Natura 2000 protected area, *Open Geosciences* **5**: 28–42. https://doi.org/10.2478/s13533-012-0120-0.

Koshnaw, R. I., Stockli, D. F., Horton, B. K., Teixell, A., Barber, D. E. and Kendall, J. J. (2020). Late Miocene deformation kinematics along the NW Zagros fold-thrust belt, Kurdistan region

of Iraq: Constraints from apatite (U-Th)/He thermochronometry and balanced cross sections, *Tectonics* **39**: e2019TC005865. https://doi.org/10.1029/2019TC005865.

Lemenkov, V. and Lemenkova, P. (2021). Using TeX Markup Language for 3D and 2D Geological Plotting, *Foundations of Computing and Decision Sciences* **46**: 43–69. https://doi.org/10.2478/fcds-2021-0004.

Lemenkova, P. (2019a). AWK and GNU Octave Programming Languages Integrated with Generic Mapping Tools for Geomorphological Analysis, *GeoScience Engineering* **65**: 1–22. https://doi.org/10.35180/gse-2019-0020.

Lemenkova, P. (2019b). Statistical Analysis of the Mariana Trench Geomorphology Using R Programming Language, *Geodesy and Cartography* **45**: 57–84. https://doi.org/10.3846/gac.2019.3785.

Lemenkova, P. (2019c). Topographic surface modelling using raster grid datasets by GMT: example of the Kuril-Kamchatka Trench, Pacific Ocean, *Reports on Geodesy and Geoinformatics* **108**: 9–22. https://doi.org/10.2478/rgg-2019-0008.

Lemenkova, P. (2020a). GEBCO Gridded Bathymetric Datasets for Mapping Japan Trench Geomorphology by Means of GMT Scripting Toolset, *Geodesy and Cartography* **46**: 98–112. https://doi.org/10.3846/gac.2020.11524.

Lemenkova, P. (2020b). Geomorphology of the Puerto Rico Trench and Cayman Trough in the Context of the Geological Evolution of the Caribbean Sea, *Annales Universitatis Mariae Curie-Sklodowska, sectio B – Geographia, Geologia, Mineralogia et Petrographia* **75**: 115–141. https://doi.org/10.17951/b.2020.75.115-141.

Lemenkova, P. (2020c). GMT Based Comparative Geomorphological Analysis of the Vityaz and Vanuatu Trenches, Fiji Basin, *Geodetski List* **74**: 19–39. https://doi.org/10.5281/zenodo.3794155.

Lemenkova, P. (2020d). NOAA Marine Geophysical Data and a GEBCO Grid for the Topographical Analysis of Japanese Archipelago by Means of GRASS GIS and GDAL Library, *Geomatics and Environmental Engineering* **14**: 25–45. https://doi.org/10.7494/geom.2020.14.4.25.

Lemenkova, P. (2020e). The geomorphology of the Makran Trench in the context of the geological and geophysical settings of the Arabian Sea, *Geology, Geophysics and Environment* **46**: 205–222. https://doi.org/10.7494/geol.2020.46.3.205.

Lemenkova, P. (2020f). Variations in the bathymetry and bottom morphology of the Izu-Bonin Trench modelled by GMT, *Bulletin of Geography. Physical Geography Series* **18**: 41–60. https://doi.org/10.2478/bgeo-2020-0004.

Lemenkova, P. (2021a). Dataset compilation by GRASS GIS for thematic mapping of Antarctica: Topographic surface, ice thickness, subglacial bed elevation and sediment thickness, *Czech Polar Reports* **11**: 67–85.

Lemenkova, P. (2021b). Geophysical Mapping of Ghana Using Advanced Cartographic Tool GMT, *Kartografija i Geoinformacije* **20**: 16–37. https://doi.org/10.32909/kg.20.36.2.

Lemenkova, P. (2021c). Mapping topographic, geophysical and gravimetry data of Pakistan – a contribution to geological understanding of Sulaiman Fold Belt and Muslim Bagh Ophiolite Complex, *Geophysica* **56**: 3–26. https://doi.org/10.5281/zenodo.5779189.

Lemenkova, P. (2021d). Submarine tectonic geomorphology of the Pliny and Hellenic Trenches reflecting geologic evolution of the southern Greece, *Rudarsko Geolosko Naftni Zbornik*

36: 33–48. https://doi.org/10.17794/rgn.2021.4.4.

Lemenkova, P. (2021e). Topography of the Aleutian Trench south-east off Bowers Ridge, Bering Sea, in the context of the geological development of North Pacific Ocean, *Baltica* **34**: 27–46. https://doi.org/10.5200/baltica.2021.1.3.

Lemenkova, P. (2021f). Using GMT for 2D and 3D Modeling of the Ryukyu Trench Topography, Pacific Ocean, *Miscellanea Geographica* **25**: 213–225. https://doi.org/10.2478/mgrsd-2020-0038.

Lemenkova, P. (2022a). Console-Based Mapping of Mongolia Using GMT Cartographic Scripting Toolset for Processing TerraClimate Data, *Geosciences* **12**: 140.

Lemenkova, P. (2022b). Handling Dataset with Geophysical and Geological Variables on the Bolivian Andes by the GMT Scripts, *Data* **7**: 74.

Lemenkova, P. (2022c). Mapping submarine geomorphology of the Philippine and Mariana trenches by an automated approach using GMT scripts, *Proceedings of the Latvian Academy of Sciences. Section B. Natural, Exact, and Applied Sciences* **76**: 258–266.

Lemenkova, P. (2022d). Seismicity in the Afar Depression and Great Rift Valley, Ethiopia, *Environmental Research, Engineering and Management* **78**: 83–96.

Lemenkova, P. (2022e). Tanzania Craton, Serengeti Plain and Eastern Rift Valley: mapping of geospatial data by scripting techniques, *Estonian Journal of Earth Sciences* **71**: 61–79.

Lindh, P. and Lemenkova, P. (2021a). Evaluation of Different Binder Combinations of Cement, Slag and CKD for S/S Treatment of TBT Contaminated Sediments, *Acta Mechanica et Automatica* **15**: 236–248. https://doi.org/10.2478/ama-2021-0030.

Lindh, P. and Lemenkova, P. (2021b). Resonant Frequency Ultrasonic P-Waves for Evaluating Uniaxial Compressive Strength of the Stabilized Slag–Cement Sediments, *Nordic Concrete Research* **65**: 39–62. https://doi.org/10.2478/ncr-2021-0012.

Lindh, P. and Lemenkova, P. (2022a). Geochemical tests to study the effects of cement ratio on potassium and TBT leaching and the pH of the marine sediments from the Kattegat Strait, Port of Gothenburg, Sweden, *Baltica* **35**: 47–59.

Lindh, P. and Lemenkova, P. (2022b). Seismic velocity of P-waves to evaluate strength of stabilized soil for Svenska Cellulosa Aktiebolaget Biorefinery Östrand AB, Timrå, *Bulletin of the Polish Academy of Sciences: Technical Sciences* **70**: 1–9.

Lindh, P. and Lemenkova, P. (2022c). Soil contamination from heavy metals and persistent organic pollutants (PAH, PCB and HCB) in the coastal area of Västernorrland, Sweden, *Gospodarka Surowcami Mineralnymi – Mineral Resources Management* **38**: 147–168.

Liu, X., Wen, Z., Wang, Z., Song, C. and He, Z. (2018). Structural characteristics and main controlling factors on petroleum accumulation in Zagros Basin, Middle East, *Journal of Natural Gas Geoscience* **3**(5): 273–281.

Lopez-Ornelas, E. and Sedes, F. (2008). Cartographic elements extraction using high resolution remote sensing imagery and xml modeling, *IGARSS 2008 - 2008 IEEE International Geoscience and Remote Sensing Symposium*, Vol. 2, pp. II–430–II–432.

Mafi-Gholami, D., Zenner, E. K. and Jaafari, A. (2022). Mapping recent (1997–2017) and future (2030) county-level social vulnerability to socio-economic conditions and natural hazards throughout iran, *Journal of Cleaner Production* **355**: 131841.

Masson, F., Anvari, M., Djamour, Y., Walpersdorf, A., Tavakoli, F., Daignières, M., Nankali, H.

and Van Gorp, S. (2007). Large-scale velocity field and strain tensor in Iran inferred from GPS measurements: new insight for the present-day deformation pattern within NE Iran, *Geophysical Journal International* **170**: 436–440. https://doi.org/10.1111/j.1365-246X.2007.03477.x.

Masson, F., Chéry, J., Hatzfeld, D., Martinod, J., Vernant, P., Tavakoli, F. and Ghafory-Ashtiani, M. (2005). Seismic versus aseismic deformation in Iran inferred from earthquakes and geodetic data, *Geophysical Journal International* **160**: 217–226. https://doi.org/10.1111/j.1365-246X.2004.02465.x.

Mokhtari, Z. and Sadeghi, B. (2021). Geochemical anomaly definition using multifractal modeling, validated by geological field observations: Siah jangal area, se iran, *Geochemistry* **81**(4): 125774. Mineral exploration: a journey from fieldwork, to laboratory work, computational modelling and mineral processing.

Mostafa Mousavi, S., Ataie-Ashtiani, B. and Mossa Hosseini, S. (2022). Comparison of statistical and mcdm approaches for flood susceptibility mapping in northern iran, *Journal of Hydrology* p. 128072.

Motaghi, K., Shabanian, E. and Kalvandi, F. (2017). Underplating along the northern portion of the Zagros suture zone, Iran, *Geophysical Journal International* **210**: 375–389. https://doi.org/10.1093/gji/ggx168.

Motaghi, K., Shabanian, E., Tatar, M., Cuffaro, M. and Doglioni, C. (2017). The south Zagros suture zone in teleseismic images, *Tectonophysics* **694**: 292–301. https://doi.org/10.1016/j.tecto.2016.11.012.

Mouthereau, F., Tensi, J., Bellahsen, N., Lacombe, O., De Boisgrollier, T. and Kargar, S. (2007). Tertiary sequence of deformation in a thin-skinned/thick-skinned collision belt: the Zagros Folded Belt (Fars, Iran), *Tectonics* **26**: TC5006. https://doi.org/10.1029/2007TC002098.

Nissen, E., Tatar, M., Jackson, J. A. and Allen, M. B. (2011). New views on earthquake faulting in the Zagros fold-and-thrust belt of Iran, *Geophysical Journal International* **186**: 928–944. https://doi.org/10.1111/j.1365-246X.2011.05119.x.

Palano, M., Imprescia, P., Agnon, A. and Gresta, S. (2018). An improved evaluation of the seismic/geodetic deformation-rate ratio for the Zagros Fold-and-Thrust collisional belt, *Geophysical Journal International* **213**: 194–209. https://doi.org/10.1093/gji/ggx524.

Paul, A., Kaviani, A., Hatzfeld, D., Vergne, J. and M., M. (2006). Seismological evidence for crustal-scale thrusting in the Zagros mountain belt (Iran), *Geophysical Journal International* **166**: 227–237. https://doi.org/10.1111/j.1365-246X.2006.02920.x.

Pavlis, N. K., Holmes, S. A., Kenyon, S. C. and Factor, J. K. (2012). The development and evaluation of the Earth Gravitational Model 2008 (EGM2008), *Journal of Geophysical Research* **117**: B04406. https://doi.org/10.1029/2011JB008916.

R Core Team (2020). R: A language and environment for statistical computing. r foundation for statistical computing, URL: https://www.R-project.org/. Vienna, Austria.

Regard, V., Bellier, O., Thomas, J., Abbassi, M. R., Mercier, J., Shabanian, E., Feghhi, K. and Soleymani, S. (2004). Accommodation of Arabia-Eurasia convergence in the Zagros-Makran transfer zone, SE Iran: A transition between collision and subduction through a young deforming system, *Tectonics* **23**: TC4007. https://doi.org/10.1029/2003TC001599.

RStudio Team (2017). Rstudio: Integrated development environment for r, https://www.RStudio.com/. RStudio Inc., Boston, MA.

Sandwell, D. T., Müller, R. D. v Smith, W. H. F., Garcia, E. and Francis, R. (2014). New global marine gravity model from CryoSat-2 and Jason-1 reveals buried tectonic structure, *Science* **7346**: 65–67. https://doi.org/10.1126/science.1258213.

Sandwell, D. T. and Smith, W. H. F. (1997). Marine gravity anomaly from Geosat and ERS 1 satellite altimetry, *Journal of Geophysical Research* **102**: 10039–10054. https://doi.org/10.1029/96JB03223.

Saura, E., Garcia-Castellanos, D., Casciello, E., Parravano, V., Urruela, A. and Vergés, J. (2015). Modeling the flexural evolution of the Amiran and Mesopotamian foreland basins of NW Zagros (Iran-Iraq), *Tectonics* **34**. https://doi.org/10.1002/2014TC003660.

Schoenbohm, L. M. (2022). 2.07 - Tectonic Geomorphology of Continental Collision Zones, *in* J. J. F. Shroder (ed.), *Treatise on Geomorphology*, 2 edn, Academic Press, Oxford, pp. 120–149.

Senturk, S., Cakir, Z. and Berk Ustundag, B. (2016). The potential of sentinel-ia interferometric sar data in monitoring of surface subsidence caused by overdrafting groundwater in agricultural areas, *2016 Fifth International Conference on Agro-Geoinformatics (Agro-Geoinformatics)*, pp. 1–4.

Sepehr, M. and Cosgrove, J. W. (2004). Structural framework of the Zagros Fold–Thrust Belt, Iran, *Marine and Petroleum Geology* **21**: 829–843. https://doi.org/10.1016/j.marpetgeo.2003.07.006.

Shi, H., Du, Z., Lu, Y., Hu, X. and Ke, X. (2009). Amery ice shelf digital elevation model from glas and gmt, *2009 Third International Symposium on Intelligent Information Technology Application*, Vol. 2, pp. 129–133.

Soleimani, M. and Jodeiri Shokri, B. (2016). Intrinsic geological model generation for chromite pods in the Sabzevar ophiolite complex, NE Iran, *Ore Geology Reviews* **78**: 138–150.

Spooner, C., Scheck-Wenderoth, M., Cacace, M., Götze, H.-J. and Luijendijk, E. (2020). The 3D thermal field across the Alpine orogen and its forelands and the relation to seismicity, *Global and Planetary Change* **193**: 103288. https://doi.org/10.1016/j.gloplacha.2020.103288.

Talebian, M. and Jackson, J. (2004). A reappraisal of earthquake focal mechanisms and active shortening in the Zagros mountains of Iran, *Geophysical Journal International* **156**: 506–526. https://doi.org/10.1111/j.1365-246X.2004.02092.x.

Tavakoli, F., Walperdorf, A., Authemayou, C., Nankal, i. H. R., Hatzfeld, D., Tatar, M., Djamour, Y., Nilforoushan, F. and Cotte, N. (2008). Distribution of the right-lateral strike–slip motion from the Main Recent Fault to the Kazerun Fault System (Zagros, Iran): Evidence from present-day GPS velocities, *Earth and Planetary Science Letters* **275**: 342–347. https://doi.org/10.1016/j.epsl.2008.08.030.

Tavani, S., Parente, M., Vitale, S., Iannace, A., Corradetti, A., Bottini, C., Morsalnejad, D. and Mazzoli, S. (2018). Early Jurassic rifting of the Arabian passive continental margin of the Neo-Tethys. Field evidence from the Lurestan region of the Zagros fold-and-thrust belt, Iran, *Tectonics* **37**: 2586–2607. https://doi.org/10.1029/2018TC005192.

Tennekes, M. (2018). tmap: Thematic Maps in R, *Journal of Statistical Software* **84**: 1–39. https://doi.org/10.18637/jss.v084.i06.

Toosi, A., Javan, F. D., Samadzadegan, F., Mehravar, S., Kurban, A. and Azadi, H. (2022). Citrus orchard mapping in juybar, iran: Analysis of ndvi time series and feature fusion of multi-source satellite imageries, *Ecological Informatics* p. 101733.

Virden, W., Habermann, T., Glover, G., Divins, D., Sharman, G. and Fox, C. (2004). Multibeam bathymetric data at NOAA/NGDC, *Oceans '04 MTS/IEEE Techno-Ocean '04 (IEEE Cat. No.04CH37600)*, Vol. 2, pp. 1159–1162 Vol.2.

Vérard, C., Hochard, C., Baumgartner, P. O., Stampfli, G. M. and Liu, M. (2015). 3D palaeogeographic reconstructions of the Phanerozoic versus sea-level and Sr-ratio variations, *Journal of Palaeogeography* **4**: 64–84. https://doi.org/10.3724/SP.J.1261.2015.00068.

Wessel, P., Luis, J. F., Uieda, L., Scharroo, R., Wobbe, F., Smith, W. H. F. and Tian, D. (2019). The Generic Mapping Tools version 6., *Geochemistry, Geophysics, Geosystems* **20**: 5556–5564. https://doi.org/10.1029/2019GC008515.

Yamini-Fard, F., Hatzfeld, D., Tatar, M. and Mokhtari, M. (2006). Microearthquake seismicity at the intersection between the Kazerun fault and the Main Recent Fault (Zagros, Iran), *Geophysical Journal International* **166**: 186–196. https://doi.org/10.1111/j.1365-246X.2006.02891.x.

Zarasvandi, A., Fereydouni, Z., Alizadeh, B., Absar, N., Dutt Shukla, A., Qaim Raza, M., Ashok, M. and Zentilli, M. (2021). Phosphogenesis in the zagros fold-thrust belt, iran: The link between the tethyan paleoenvironment and phosphate ore deposition, *Ore Geology Reviews* **139**: 104563.

Received: *2022-04-01*

Reviewed: *2022-05-13 (J. Pluto-Kossakowska); 2022-06-20 (undisclosed name)*

Accepted: *2022-06-20*